



LAWRENCE
LIVERMORE
NATIONAL
LABORATORY

Structure and Composition of Cu Doped CdSe Nanocrystals Using Soft X-ray Absorption Spectroscopy

R. W. Meulenberg, T. van Buuren, K. M. Hanif, T. M. Willey, G. F. Strouse, L. J. Terminello

June 9, 2004

Nano Letters

Disclaimer

This document was prepared as an account of work sponsored by an agency of the United States Government. Neither the United States Government nor the University of California nor any of their employees, makes any warranty, express or implied, or assumes any legal liability or responsibility for the accuracy, completeness, or usefulness of any information, apparatus, product, or process disclosed, or represents that its use would not infringe privately owned rights. Reference herein to any specific commercial product, process, or service by trade name, trademark, manufacturer, or otherwise, does not necessarily constitute or imply its endorsement, recommendation, or favoring by the United States Government or the University of California. The views and opinions of authors expressed herein do not necessarily state or reflect those of the United States Government or the University of California, and shall not be used for advertising or product endorsement purposes.

Structure and Composition of Cu Doped CdSe Nanocrystals Using Soft X-ray Absorption Spectroscopy

Robert W. Meulenberg^{1,*}, Tony van Buuren¹, Khalid M. Hanif²,
Trevor M. Willey¹, Geoffrey F. Strouse^{3,*}, Louis J. Terminello¹

¹Lawrence Livermore National Laboratory,
Livermore CA 94550

²Optical Sciences Division, Naval Research Laboratory,
Washington, D.C. 20375

³Department of Chemistry, Florida State University,
Tallahassee FL 32316

* meulenberg1@llnl.gov

* strouse@chem.fsu.edu

September 9, 2004

Abstract

The local structure and composition of Cu ions dispersed in CdSe nanocrystals is examined using soft x-ray absorption near edge spectroscopy (XANES). Using Cu *L*-edge XANES and X-ray photoelectron measurements (XPS), we find that the Cu ions exist in the Cu(I) oxidation state. We also find that the observed Cu *L*-edge XANES signal is directly proportional to the molar percent of Cu present in our final material. Se *L*-edge XANES indicates changes in the Se density of states with Cu doping, due to a chemical bonding effect, and supports a statistical doping mechanism. Photoluminescence (PL) measurements indicate the Cu ions may act as deep electron traps. We show that XANES, XPS, and PL are a powerful combination of methods to study the electronic and chemical structure of dopants in nanostructured materials.

1 INTRODUCTION

The study of nanostructured particles has received much attention in the last decade due to unique physical properties which are strongly dependent on the

spatial dimensions of the particles. [1] For particle radii close to the Bohr exciton of the material, quantum confinement effects dominate the optical and electronic properties of these particles. [2] These systems have been targeted for uses in many types of applications, including electronic, magnetic, and optical devices [3, 4, 5] as well as biomedical tagging.[6] In addition, recent advances in nanoparticle fabrication have allowed researchers to produce well formed nanostructured particles doped with transition metal ions. [7] These studies lead researchers to believe that the next magnetic storage devices can be fabricated using doped nanoparticles. A large obstacle, however, towards these goals is understanding the chemistry and physics of the impurity ion in a nanoparticle lattice and its impact on useful and desirable properties.

To understand the effect an impurity or dopant ion has on the structural and electronic properties in a quantum dot, one must first examine how these types of effects are understood in its corresponding bulk lattice. For our study of Cu ion doping in a CdSe nanoparticle lattice, we begin by examining Cu doped into bulk CdSe. Experimentally, CdSe:Cu bulk has been studied previously and been targeted for uses in photovoltaics; many studies have been aimed at understanding the defect and transport properties of such materials. [8, 9, 10, 11] Several of these studies have observed that Cu in CdSe can act as both an acceptor and donor, with reports of Cu acting as a deep electron acceptor about 0.5 eV below the conduction band minimum (CBM). In addition, many computational studies have been recently targeted on transition metal doped semiconductors, with doping described in terms of the "doping pinning rule". Zhang *et al.* have established that doping in semiconductors can be explained by considering the valence band maximum (VBM) offset with respect to a $p(n)$ like pinning energy. This has established a simple, yet effective, way to determine the relative carrier concentration if a system can be doped. [12] As predicted by Zhang *et al.*, CdSe can easily be n doped, and lightly p doped. [13] The prediction of n type doping is consistent with the observation of deep levels below the CBM as mentioned above. Finally, Wei *et al.* have predicted the formation of Cu substitutional defects in CdX (where X = S, Se, Te) to be energetically favorable. [14] In addition, they predict a lattice compression with Cu single ion substitution, as expected from the smaller Cu ion. With this understanding of CdSe:Cu bulk, we will exploit it in our efforts in studying CdSe:Cu nanoparticles.

In this manuscript, we will discuss the properties of a new Cu doped CdSe semiconductor nanocrystal using many physical characterization techniques including soft x-ray absorption near edge spectroscopy (XANES), x-ray photoelectron spectroscopy, optical spectroscopy (absorption and photoluminescence), powder x-ray diffraction, and transmission electron microscopy. We will show how in particular how XANES is a powerful tool to understating oxidation states in these doped particles. XANES is an ideal tool to study chemical impurities in nanoparticle owing to its inherent elemental specificity. A knowledge of the oxidation state of a dopant ion in a nanocrystal lattice can allow one access to the number of electrons per atom which will be useful when fabricating devices based on electron spin manipulation.

2 EXPERIMENTAL

2.1 Synthesis

2.1.1 Materials

The $(\text{Li}_4)[\text{Se}_4\text{Cd}_{10}(\text{SPh})_{16}]$ clusters were prepared according to literature methods. [15] $\text{Cd}(\text{NO}_3)_2 \cdot 4\text{H}_2\text{O}$ (Strem), $\text{Cu}(\text{NO}_3)_2 \cdot 2\text{H}_2\text{O}$ (Fisher), selenium powder (~ 200 mesh, Aldrich), thiophenol (Aldrich), triethylamine (Fisher), Methanol (ACS Grade), Acetonitrile (HPLC Grade), hexadecylamine (90 %, Acros), pyridine (EM Science), and hexanes (Fisher) were used as supplied.

2.1.2 Synthesis of $[\text{Cu}_4(\text{SPh})_6](\text{TMA})_2$

$[\text{Cu}_4(\text{SPh})_6](\text{TMA})_2$ was synthesized by combining a solution of (15.8 g, 68 mmol) $\text{Cu}(\text{NO}_3)_2 \cdot 4\text{H}_2\text{O}$ in 70 mL methanol to a stirred room temperature solution of (20.0 g, 182 mmol) benzenethiol and (18.5g, 182 mmol) triethylamine in 40 mL methanol. To this mixture, a solution of (8.4g, 77 mmol) tetramethylammonium chloride (TMACl) in 40mL methanol was added, and the product was then allowed to crystallize at 0 °C producing a yellow solid. The solution was filtered, washed with cold methanol and vacuum dried. The sample was characterized by electrospray ionization mass spectrometry with a parent ion peak for $[\text{Cu}_4(\text{SPh})_6]^{2-}$ observed at 454.7 m/z.

2.1.3 Synthesis of $\text{Cd}_{1-x}\text{Cu}_x\text{Se}$ Nanocrystals

Synthesis of $\text{Cd}_{1-x}\text{Cu}_x\text{Se}$ quantum dots was performed by using a parallel plate methodology by mixing ~ 1.200 g of $(\text{Li}_4)[\text{Se}_4\text{Cd}_{10}(\text{SPh})_{16}]$ and various concentrations of $(\text{TMA}_2)[\text{Cu}_4(\text{SPh})_6]$, [0.100g, 0.200 g, 0.300 g, 0.400g, 0.500g, 0.600g, 0.700g, and 0.900g] in 9 different reaction vials. The materials were placed under vacuum and to these flasks about 35mL aliquots of n-hexadecylamine (HDA) was added at ~ 100 °C. Growth of the doped nanocrystals was accomplished by heating the solution to ~ 250 °C at a rate of ~ 20 °C/hour. Nanocrystal growth is followed by monitoring the optical absorption spectral linewidth to ensure a narrow particle size dispersion. Growth of the doped quantum dots was halted when they approached ~ 40 Å in size. The quantum dots were isolated from excess HDA and recapped with pyridine according to literature methods. [7] These materials were stripped and recapped with pyridine twice to ensure any Cu that is not part of the quantum dot is removed.

2.2 Materials Characterization

2.2.1 Soft x-ray absorption near edge spectroscopy

Soft x-ray absorption near edge spectroscopy (XANES) spectra were acquired at the undulator beamline 8.0.1 at the Advanced Light Source at the Lawrence Berkeley National Laboratory. The nanoparticles were pressed into carbon tape, and the spectra were taken on these powder samples. XANES experiments

were conducted using the total electron yield (TEY) detection method where the total photocurrent is measured as the photon energy is scanned through the absorption edges. The experimental energy resolution was ~ 0.20 eV at the copper *L*-edge. The incident photon flux is measured with a highly transmissive gold grid and all spectra are normalized to the current from the gold grid. Cu *L*-edge spectra were calibrated to the CuO peak at 931 eV. [18] All spectra were recorded at room temperature and base pressures of less than 8×10^{-9} torr. The relatively high pressure in these experiments are due to sample outgassing from any residual solvent left in the nanoparticles in the cleaning process.

2.2.2 X-ray photoelectron spectroscopy

X-ray photoelectron spectroscopy (XPS) measurements were performed on a Kratos Axis Ultra X-ray photoelectron spectrometer with an Al- $K\alpha$ source. Samples were dissolved in hexanes and drop cast on glass slides (because of the insulating substrate, a flood gun was used to compensate for charging of the materials). The C 1s peak was used to calibrate the spectral position due to charge induced shifting in the observed XPS pattern. All measurements were performed below 1×10^{-8} Torr.

2.2.3 Transmission electron microscopy

Transmission electron microscope measurements were performed on a JEOL 2010 High Resolution microscope. Samples were dissolved in toluene and deposited on Nickel holey carbon grids. The TEM has a resolution of 2 Å at 200 kV. TEM images were used to determine the size and size distributions of the particles.

2.2.4 Powder X-ray diffraction

Powder x-ray diffraction measurements (p-XRD) were performed on a Scintag X2 diffractometer with a Cu $K\alpha$ source ($\lambda = 1.5418$ Å). Si powder was used as an internal standard. The sharp peaks in the p-XRD at 1.638, 1.920, and 3.136 Å are due to the Si standard.

2.2.5 Optical measurements

UV-Visible solution absorption measurements were performed at room temperature on a CARY 50 Bio UV-VIS spectrophotometer. Photoluminescence measurements were performed in toluene solutions at room temperature on a CARY Eclipse fluorescence spectrophotometer using an excitation energy of 490 nm.

2.2.6 Inductively-Coupled Plasma Atomic Emission Spectroscopy

Elemental analysis of the obtained materials was performed using a Thermo-Jarrell Ash IRIS Inductively-Coupled Plasma Atomic Emission Spectropho-

tometer. All samples were dissolved in 2 % HNO₃ solution. The Cd and Cu standards used in these measurements were purchased from High Purity Standards. The Cd concentration was monitored using the 214.438 and 226.5 nm atomic emission lines. The Cu concentration was determined using the 223.008, 224.700 and 327.396 nm atomic emission lines of Cu. An average of three runs were taken for each element with an error of < 5%.

3 RESULTS AND DISCUSSION

3.1 Determination of Nanoparticle Size and Doping Levels

The quantum dots exhibit a narrow band edge absorption that ranges from ~540 - 560 nm (2.2-2.3 eV) consistent with the absorption of 38 - 42 Å particles as seen in Figure 1. TEM images corroborate that these particles are ~40Å in size and have a ~7% size distribution. Observable lattice fringes in the TEM images indicate these materials are crystalline with ABCAB stacking that is consistent with that of a cubic structure. Although stacking faults are observed in the TEM images of some of the quantum dots, the vast majority of quantum dots have no stacking faults or glide plane defects.

For determination of the amount of Cu dopant present, elemental analysis was performed. However, as it is well known that nanocrystals can readily trap dopants on the particle surface, it is necessary to establish to what degree the *core* of the particle is doped. To this end, the elemental analysis was performed prior to and after recapping with pyridine, as pyridine has been previously shown to be effective in removing surface adsorbed species in nanocrystals. The pyridine recapping showed very little difference in the amount of copper relative to cadmium in the samples (see Supplemental Figure 1), indicative of a system where most of the chemical dopant is situated in the core of the particle. To estimate the number of Cu atoms that are present in the different doped systems, we used the DIAMOND crystallography package. Using DIAMOND, we are able to calculate that a 40 Å quantum dot (the size in this study) has approximately 1177 atoms of which 577 would be Cd atoms. The samples synthesized in this study had doping levels of 5.4%, 6.6%, 9.9%, 13.1%, 15.4% Cu. Therefore the quantum dots would on average have 19, 31, 38, 57, 66, 89, 117, and 118 Cu atoms within each dot respectively.

3.2 Proof of Core Doping of Cu in CdSe Nanocrystals

As evidenced from the ICP-AE measurements, the Cu dopants show very little evidence for surface adsorption which indicates core doping of the nanocrystal. Controlling chemical doping in nanoparticles allows the fine tuning of the lattice parameters which can be useful in methods to control the properties of the nanoparticles. For instance, one can selectively change the core properties of CdSe by introducing two different dopant ions, Co [7] and Eu [16], as Co will

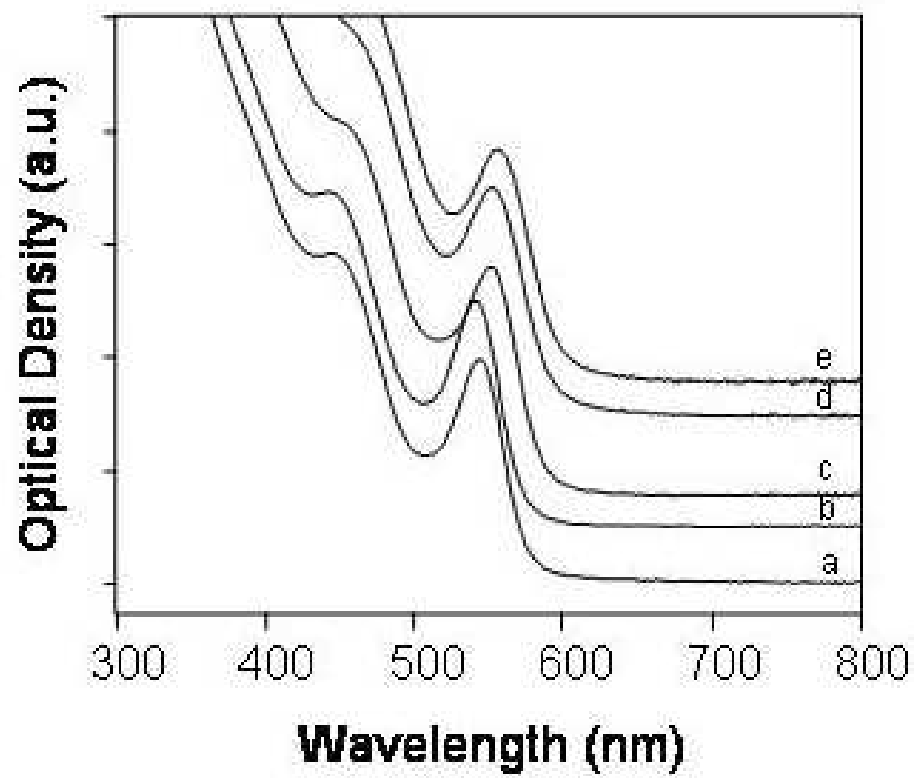


Figure 1: Optical absorption spectra of (a) 5.5, (b) 6.6, (c) 9.9, (d) 13.2, and (e) 15.2 mole percent Cu doped CdSe QDs.

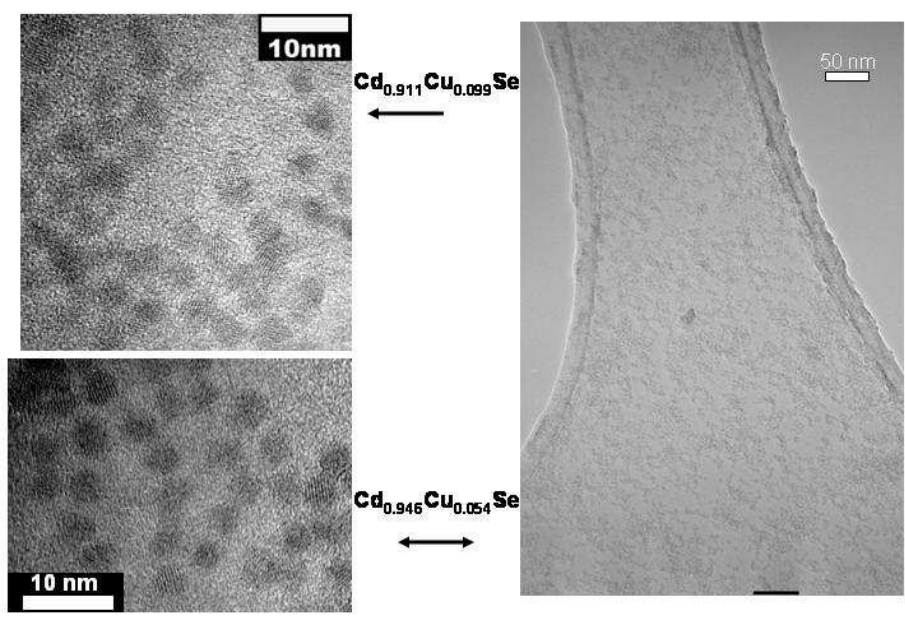


Figure 2: TEM images of deposited arrays of $\text{Cd}_{1-x}\text{Cu}_x\text{Se}$ QDs.

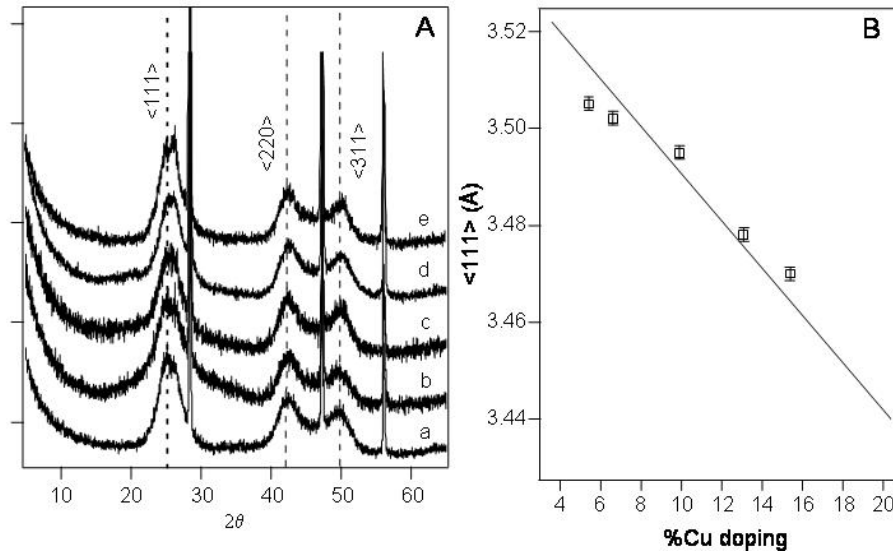


Figure 3: (A) Powder X-ray diffraction spectra of (a) 5.5, (b) 6.6, (c) 9.9, (d) 13.2, and (e) 15.2 mole percent Cu doped CdSe QDs. The large narrow lines are due to the Si standard. (B) Shift in $\langle 111 \rangle$ lattice parameter as a function of molar percent Cu. The line is a guide for the eye.

cause a significant lattice contraction due to its smaller ionic radius while Eu will cause a lattice expansion due to its larger ionic radius (when compared with Cd). This effect is well known through the phenomenological Vegard's Law, which is a predictive tool for the structural effects of dopants. Therefore, by plotting the change in lattice parameter (from p-XRD) as a function of dopant concentration, we can study structural effects of the chemical dopants in CdSe nanocrystals.

Although undoped CdSe nanocrystals tend to have a wurtzite crystal structure at ambient conditions, [17] we see from Figure 3a that the structure of the $\text{Cd}_{1-x}\text{Cu}_x\text{Se}$ nanocrystals synthesized in this manuscript is zinc blende. As the energy difference between wurtzite and zinc blende crystal structures is ~ 70 meV, it is not inconceivable that the presence of Cu ions create enough of a driving force to form a zinc blende as opposed to the typical wurtzite structure. The powder diffraction of the doped samples exhibit three peaks that can be assigned to $\langle 111 \rangle$, $\langle 220 \rangle$ and $\langle 311 \rangle$ reflections of the zinc blende structure and are Scherrer broadened from the finite crystallite size. Inspecting Figure 3b, it is seen that the $\langle 111 \rangle$ peak shifts to smaller d-spacing as the doping level is increased in accordance with Vegard's law. The p-XRD data, along with the ICP-AE data, is consistent with increased levels of Cu cations being incorporated within the lattice of the host material and the compression in the lattice parameters are consistent with the smaller Cu ion substituting in a single ion

doping mechanism for the larger Cd ion.

3.3 X-ray Photoelectron Spectroscopy

To probe the chemical environment of the Cu dopant ion in the CdSe nanoparticle, we first used x-ray photoelectron spectroscopy (XPS). XPS analysis of Cu $2p$ spectra can be interpreted in terms of a charge transfer model in which two different final states result in "well-screened" and "poorly-screened" or "satellite" peaks. [19] Formally, Cu(I) with an initial state of $3d^{10}$ exhibits only a well-screened peak as the $3d$ orbital is completely full. Previous experiments have shown Cu(I) to have a well-screened Cu $2p_{2/3}$ peak at 932.4 ± 0.2 eV with no satellite peaks. [19] Experimentally, we have found the Cu $2p_{3/2}$ peak is seen at 932.3 eV, with the $2p_{1/2}$ at 952.1 eV for our $\text{Cd}_{1-x}\text{Cu}_x\text{Se}$ QD samples (see Supplemental Figure 2). The spin-orbit splitting observed is 19.8 eV which closely matches the reported value of 19.6 eV. [20] The lack of an observed satellite peak rules out the possibility for Cu(II) in these samples, and the well-screened peak is indicative of Cu(I). [19] This approach has been applied recently to Cu based insulators, where the observation of a well-screened $2p_{2/3}$ peak lead the authors to assign a charge state of +1 to their Cu materials. [21] However, it should be noted that the XPS spectra of both Cu(I) and Cu(0) are similar as both have a filled $3d$ orbital and the Cu $2p_{3/2}$ peak differs by only 0.1 eV. [22] X-ray absorption spectroscopy can be used to further confirm the difference between the Cu(I) or Cu(0). In the next section, we will detail our x-ray absorption measurements of these materials.

3.4 Soft X-ray Absorption Spectroscopy

3.4.1 Cu L -edge

Another method to probe the oxidation state of the doped ions is soft x-ray absorption near edge spectroscopy (XANES). For Cu L -edge spectra, the formal electronic transition can be denoted as an electron from the occupied $2p$ levels to the final states of s or d character due to dipole selection rules. In the most simplified terms, for a Cu atom the $\Delta l=-1$ channel is 10 times weaker than the $\Delta l=+1$ channel [23], and the measured edge can generally be thought as the mapping out of the Cu d partial density of states (PDOS). [24] The shape and position of the Cu L_3 absorption edge can vary greatly as the oxidation state of the Cu atom changes. For instance, the L_3 edge of a Cu(II) ion (in the form of CuO) has a very strong peak at 931.3 eV. This peak is not a DOS feature, as the Cu $2p_{3/2}$ binding energy is 932.3 eV, but rather has been identified as a core-exciton. [18] Figure 4 plots the Cu L_3 absorption edges of Cu metal (formally Cu(0)) deposited on Si, CuSe (formally Cu(II)), CuI (formally Cu(I)), $[\text{Cu}_4(\text{SC}_6\text{H}_5)_6](\text{NMe}_4)_2$ cluster used to dope the nanoparticles (formally Cu(I)), and a 15.2% Cu doped CdSe nanoparticle sample. Qualitatively, due to the similarity in the Cu L -edge XANES spectra, it can be stated that the $[\text{Cu}_4(\text{SC}_6\text{H}_5)_6](\text{NMe}_4)_2$ cluster and the Cu doped CdSe nanoparticle sample are

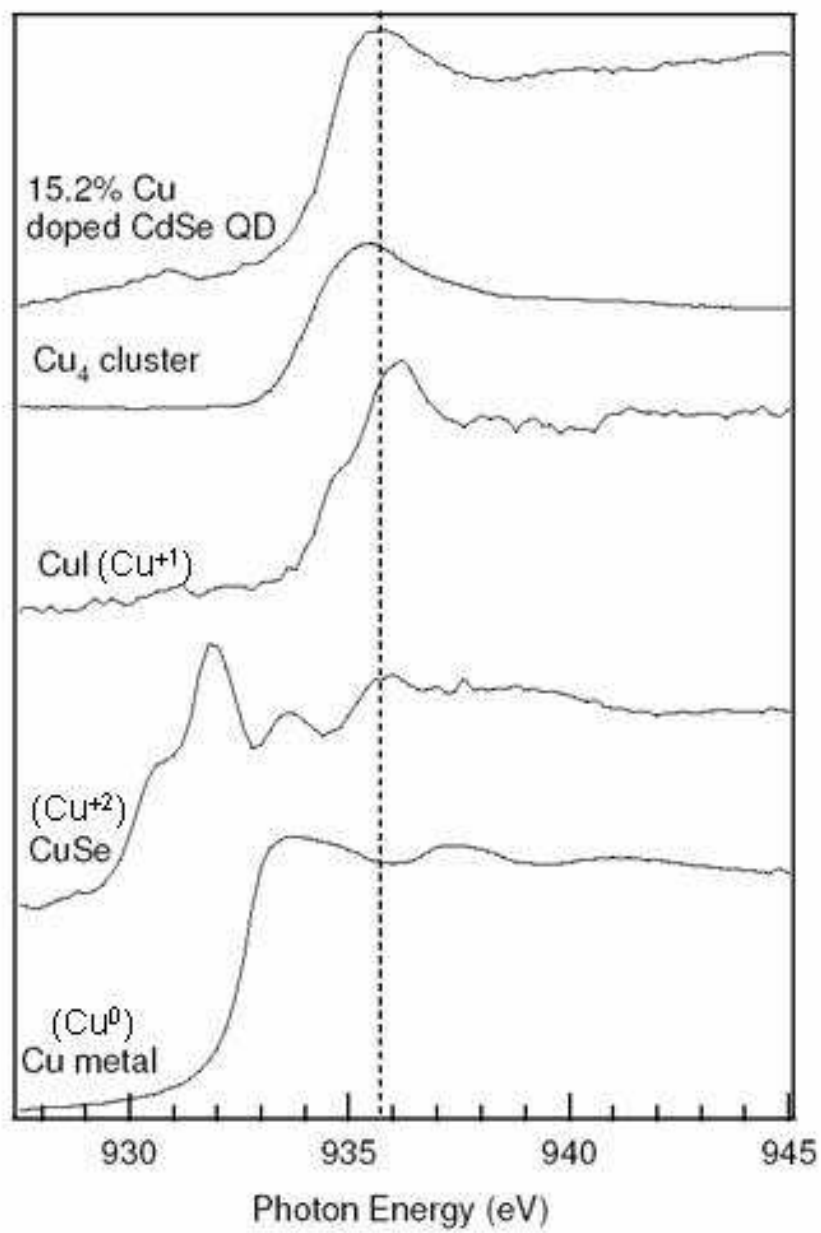


Figure 4: Cu L -edge XANES spectra of samples studied in this manuscript. The spectra are normalized to unity at the L_3 peak maximum.

structurally and chemically similar. Both samples show the Cu L_3 absorption at ~ 934 eV with the Cu L_2 peak at ~ 954 eV corresponding to a spin-orbit splitting of ca. 20 eV, as previously reported. Interestingly, there exists a small chemical shift effect between the $[\text{Cu}_4(\text{SC}_6\text{H}_5)_6](\text{NMe}_4)_2$ cluster and the Cu doped CdSe nanoparticle sample of ~ 0.2 eV, which could be indicative of the Cu atoms going from a sulfur environment in the cluster to a selenium environment in the nanoparticle. The CuI standard also has an L_3 absorption at ~ 934.5 eV, with a shoulder at ~ 933 eV which has been previously been attributed to a valence exciton. [25] The $[\text{Cu}_4(\text{SC}_6\text{H}_5)_6](\text{NMe}_4)_2$ cluster and the Cu doped CdSe nanoparticle samples show no evidence for the valence exciton shoulder, although the energy position of the L_3 peak is close to the value observed for the CuI standard. The Cu metal standard has an L_3 absorption edge energy of ~ 932.5 eV. The CuSe standard has an absorption at ~ 930 eV, which is the signature feature of Cu(II) in CuX samples (where X = O, S, Se). It is worthwhile to note that the $[\text{Cu}_4(\text{SC}_6\text{H}_5)_6](\text{NMe}_4)_2$ cluster shows no evidence for CuO and Cu:CdSe sample shows minimal CuO contamination, indicating the samples are not heavily oxidized. In addition, Cd and/or Se oxidation is not a factor as we saw no XPS evidence for Cd or Se oxides. Most importantly, however, is the distinct chemical shift in the XANES spectra between Cu metal and CuI, allowing, without question, assignment of the oxidation state of the Cu in our CdSe nanocrystal to be Cu(I).

Although we have identified that the oxidation state of the Cu ions in the highest doped CdSe sample is in fact Cu(I), we have not yet examined if there is an oxidation state dependence on dopant concentration. Figure 5a plots a series of Cu doped CdSe nanocrystals ranging from Cu ion molar percent of ~ 2 up to ~ 15 . For plotting purposes in Figure 5a, a previously reported protocol was used [26] for normalization of all the spectra by subtracting a linear background below the threshold and setting the L_3 peak maximum to unity. The general trends of the data are (a) the L_3 -edge stays at nearly a constant energy through the doping range and (b) there exists changes in the intensity of the L_3 peak in the unnormalized spectra. The observation of a constant L_3 -edge energy indicates that the oxidation state of the Cu ions in the CdSe nanocrystal is Cu(I) through all doping concentration studied. This constant oxidation state is indicative of the Cu ion being a highly localized defect with very little charge transfer to the host lattice. The observation of a doping concentration L_3 peak intensity indicates that not only can the XANES spectra identify the oxidation state of the dopant ion, but also can provide information on the relative amount of dopant present in the material. By taking spectra in the TEY method and ensuring that our prepared samples are sufficiently thick (> 1 micron), we can infer that the integrated intensity of the L_3 peak is proportional to the amount of species present in the material. In addition, we also are neglecting any white line enhancement due to charge transfer, which is reasonable based on the constant energy position of all the doped samples. In Figure 5b, we have plotted the integrated intensity of the Cu L_3 peak as a function of molar percent Cu. A fairly strong correlation is observed, allowing us to affirm that the Cu L -edge XANES spectra is not only a good indicator of the oxidation state of a chemical

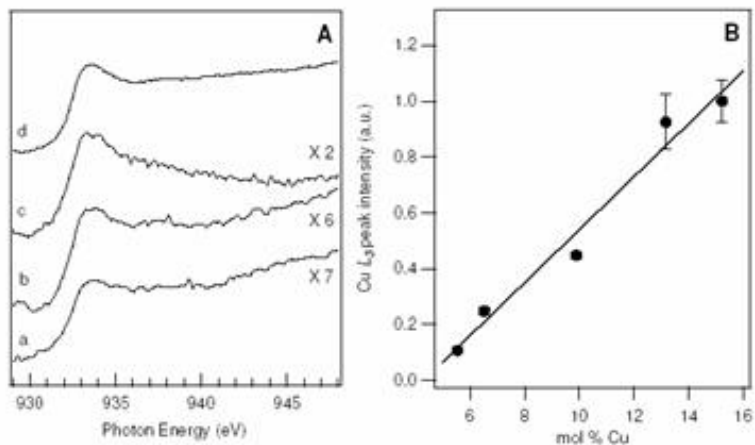


Figure 5: (A) Cu *L*-edge XANES normalized spectra of (a) 5.5, (b) 9.9, (c) 13.2, and (d) 15.2 mole percent Cu doped CdSe QDs. (B) Cu *L*₃-peak intensity as a function of molar percent Cu. The line is a guide for the eye.

dopant, but also the amount present in the host material as derived from peak intensities.

3.4.2 Se *L*-edge

From XPS and Cu *L*-edge XANES measurements, we have established that Cu ions dispersed in CdSe nanoparticles exist in a +1 oxidation state. These results are not too surprising, as the Cu cluster used to dope the nanoparticle has Cu ions in a +1 oxidation state. Also, from the pXRD results, we have proof of core doping of the Cu ions through a single ion doping mechanism. However, inspection of Fig. 4 could arise such a question like "Why the Cu₄ cluster and Cu dopant in the CdSe nanoparticle have very similar XANES spectra"? The spectral similarities may indicate that Cu ions are not statistically doping into the CdSe lattice, although the pXRD has shown statistical doping, but are doping as a Cu₄ cluster. Using Se *L*-edge XANES, we will be able to analyze the doping mechanism and examine the validity of using Vegard's law in nanocrystalline systems.

With regards to Cu₄ doping in a CdSe nanoparticle, there are some structural considerations when proposing such a drastic doping condition (see Figure 6). First, the radius of a Cu₄ cluster is ~0.25 nm while the ionic radius of a Cd²⁺ ion is ~92 pm meaning that the Cu₄ cluster cannot substitute for a single Cd site. More likely is the substitution of a tetrahedral fragment of [CdSe₄]⁶⁻, as it would be amendable to a cluster as large as Cu₄ (and lead to

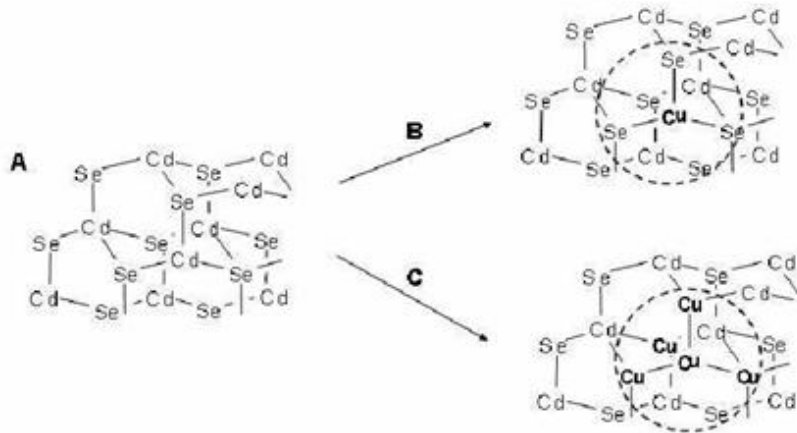


Figure 6: Cu substitutional possibilities in CdSe (A) CdSe lattice fragment (B) Single Cu ion substitution for Cd site. Notice nearest neighbors are Se. (C) Cu_4 cluster substitution into CdSe lattice. Notice nearest neighbor is Cd.

the same charge imbalance scenario in the single ion doping case). With this knowledge, it is evident that the local environment between a single Cu ion and a Cu_4 cluster in the CdSe lattice will be different (i.e. one will have a Se neighbor, one will have a Cd neighbor). With this information, we will examine the Cu site substitution in CdSe QDs using Se L -edge XANES.

XANES spectra at the Se L -edge can be a valuable tool to probe the local bonding environment in a solid state material. Se L -edge XANES consists of peaks at ~ 1434 eV and ~ 1474 eV due to the spin-orbit split L_3 and L_2 transitions. The formal transition involved the promotion of a $2p$ core electron into s and d derived empty states. In bulk CdSe, the valence band is comprised mainly from Se $4p$ orbitals, with the conduction band formed from Cd $5s$ states. [27] In a CdSe nanocrystal, the valence band is formed from Se $4p$, with a contribution from Cd $4p$ orbitals. The empty states are comprised of both Se $5s$ and $4d$ orbitals, with the conduction band minimum comprised primarily of Cd $5s$ states, with a slight contribution from Se $5s$ states. [28] Therefore, changes in the nanocrystal orbital hybridization (i.e. substituting a Cd ion for a Cu ion) will have an impact on the nanocrystal electronic structure and will be evident in the XANES spectra. Although both the L_3 - and L_2 -edges are observable, the L_2 edge features occur in the background of the L_3 -edge features and the L_3 edge is more intense by about a factor of two. Because of these differences, the L_3 -edge will be the focus of our analysis. Se L -edge spectra for undoped CdSe, and 9.9, 13.2, and 15.2 mole percent Cu doped CdSe is plotted in Figure 7a. A shoulder at ~ 1419 eV in the Se L_3 -edge has previously been attributed to Se d hybridization with $\text{Se}(p)\text{-Mn}+$ anti-bonding type orbitals. [29] The shoulder

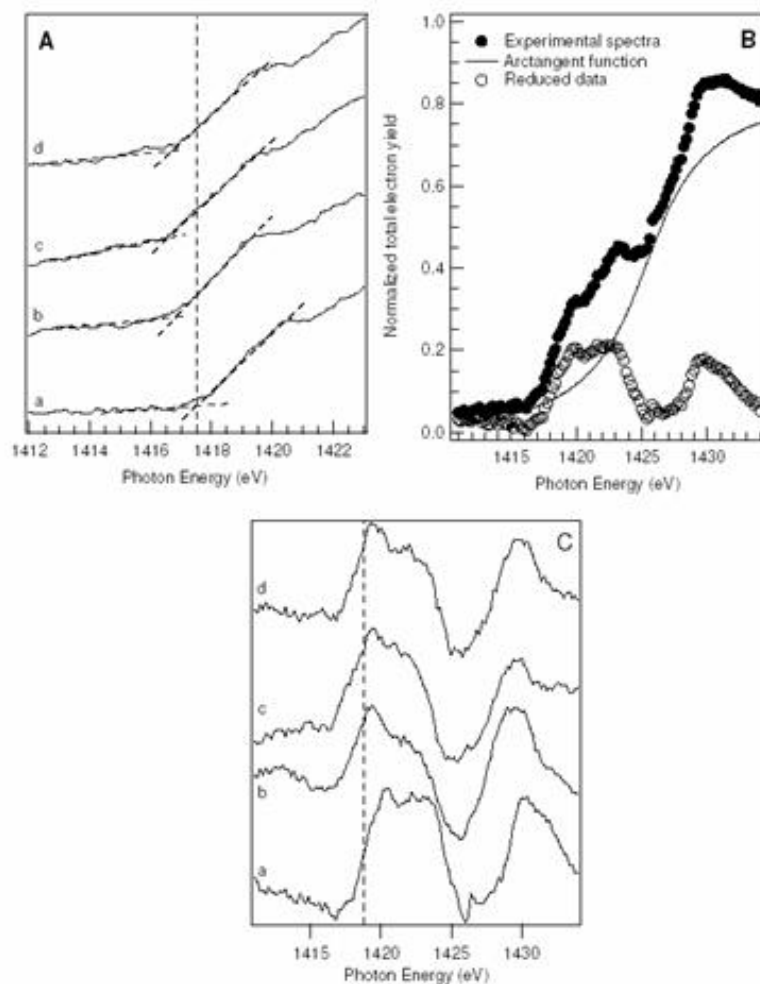


Figure 7: Normalized total electron yield (A) Se L_3 -edge XANES spectra of (a) undoped CdSe QD, (b) 9.9, (c) 13.2, and (d) 15.2 mole percent Cu doped CdSe QDs. (B) Example of reduced Se L_3 -edge spectra (see text for details). (C) Reduced Se L_3 -edge XANES spectra of (a) undoped CdSe QD, (b) 9.9, (c) 13.2, and (d) 15.2 mole percent Cu doped CdSe QDs.

position and intensity has been shown to vary as the metal cation is varied, indicative that this shoulder is a strong indicator of the local environment around the Se atoms. A peak at ~ 1424 eV is related to the main d band of the Se PDOS while in a previous study, a peak at 1430 eV has been assigned to Se d hybridization with Cu and In p states. [29] As seen from Figure 7a, upon addition of Cu to the CdSe QD, a shift in the absorption onset of 0.7-0.8 eV is seen. It is worthwhile to note that the peak at ~ 1430 eV appears to show a chemical shift effect, but because it is not as obvious as the shift in the absorption onset we will not discuss it further. To gain more quantitative information from the Se XANES spectra, we show background subtracted data in Fig. 7b and c. The broadened step absorption, μ , can be approximated by an arctangent function with a Lorentzian half-width, Γ , [29]

$$\mu = \mu_o \left[\frac{\pi}{2} + \arctan \frac{2(h\omega - E_o)}{\Gamma} \right] \quad (1)$$

, where μ_o is the baseline absorption coefficient, $h\omega$ is the inflection point energy, and E_o is the Se L -edge absorption energy. The L_3 absorption edge shifts to lower energy by 0.6-0.7 eV when going from a undoped CdSe particle to a Cu doped CdSe particle, consistent with the shifts observed in the unnormalized spectra in Figure 7a. This is consistent with the Se environment effectively becoming "oxidized" as the more electronegative Cu ion is substituted for a Cd site in the CdSe lattice. Also, as stated above, since the onset/peak at 1420 eV can be attributed to Se d hybridization M^{n+} orbitals, going from $M = \text{Cd}$ to $M = \text{Cu}$ would affect the DOS features at the absorption onset and result in the observed shift. Because the Se L - edge data shows a distinct chemical shift upon addition of Cu to the CdSe nanoparticle, this provides fairly strong evidence for a single ion doping mechanism as seen in Figure 6b, since cluster doping would have a less drastic effect on the local Se environment. This affirms the Vegard's law analysis from the pXRD spectra should be valid for nanocrystalline systems.

3.4.3 Steady State Photoluminescence

In the previous sections, we have identified that Cu dopants in CdSe nanocrystals can be tuned between 5-15 mole percent, exist in a +1 oxidation state, and dope according to a statistical substitutional mechanism. Interestingly, the fact that the Cu ion exist in a +1 oxidation state indicate that the CdSe lattice should exhibit unique optical properties, as the nanocrystal itself will have an effective charge, or induce defects due to self compensation to achieve charge stability. A method to probe defects in the nanocrystal is photoluminescence (PL) spectroscopy. PL spectroscopy has been used heavily to probe quantum confinement effects in nanostructured materials. [30] For CdSe, the PL results can be generalized as PL originating from two different states: "band-edge" (BE) PL Stokes shifted from the optical absorption onset dominated by inhomogeneous broadening due to sample size dispersity and a lower energy PL peak postulated to arise from sub-gap trap states. The origin of this low energy PL has been attributed to surface states of the nanoparticle which can act as

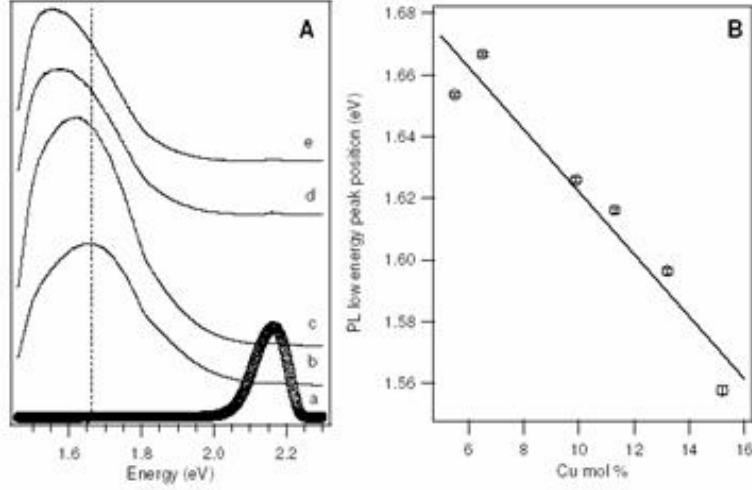


Figure 8: Normalized PL spectra of (a) undoped CdSe QD and (b) 5.5, (c) 9.9, (d) 13.2, and (e) 15.2 mole percent Cu doped CdSe QDs. (B) Cu low energy PL peak position as a function of molar percent Cu. The error bars are within the experimental points. The line is a guide for the eye.

electron or hole acceptors and radiatively recombine. [31] By studying the effect of the PL as an impurity atom (i.e. a donor or acceptor) is introduced to the nanocrystal, we can begin to understand the effect the impurity ion has on the overall nanoparticle electronic structure.

Figure 8a plots the PL spectra for a series of Cu doped CdSe nanoparticles. The $x = 0$ PL spectra consists of strong BE PL at ~ 2.15 eV with a small contribution from the low energy PL, as previously reported. [17] General inspection of the data shows that for the doped samples, the BE PL is quenched and exhibits a strong low energy PL. As the doping concentration is increased, the low energy PL shifts to lower energy. The 5.5 % Cu doped CdSe sample exhibits a very weak BE PL that occurs at 2.15 eV with a stronger low energy peak at 1.65 eV (a difference of 0.5 eV). As doping concentration increases, the BE PL remains quenched and the low energy PL band continues to redshift. At the largest Cu doping percentage, the differences between the BE PL and the low energy PL is 0.62 eV. This is plotted in Figure 5b, where we observe a strong correlation between the low energy PL peak and Cu mole percent. It should be noted that the low energy PL intensity does not follow a very strong correlation with Cu concentration, indicating the this peak is related to the inclusion of Cu into the CdSe lattice, but the peak intensity is not necessarily indicative of the

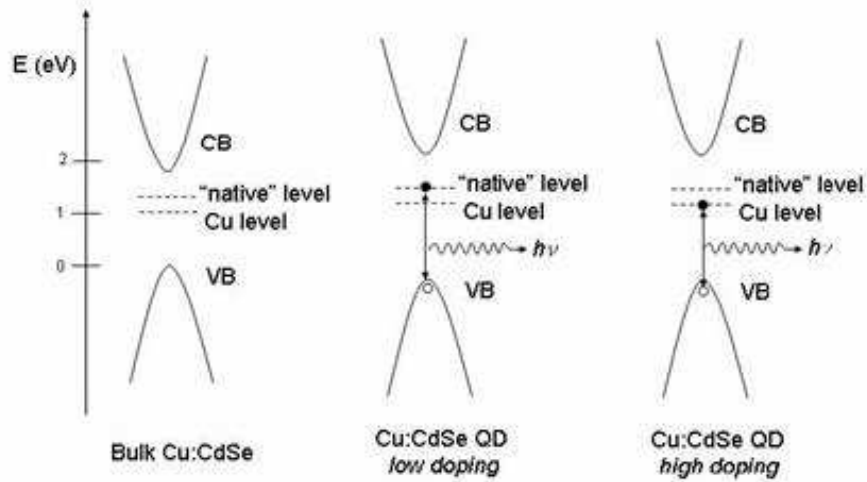


Figure 9: Schematic band diagrams illustrating effects of Cu ions on the band structure of CdSe bulk and QDs.

amount of Cu in the lattice. As stated above, typical analysis of CdSe nanocrystal PL spectra has been to assign the low energy PL to surface levels. However, comparison of both undoped CdSe NC and Cu:CdSe NC PL may provide more insight into the PL mechanism in nanostructures. The room temperature PL measurements in this study can rule out the possibility for shallow donors or acceptors contributing to the phenomenon seen in Figure 8 due to the thermal energy being much larger than the shallow state binding energy. More likely, the behavior occurs from deep sub-gap trap levels, and the data in Figure 8b indicates that the Cu doping has a significant effect on the deep level contribution to the PL. It has been proposed that native CdSe contains deep levels ~ 1.3 eV above the valence band maximum (or ~ 0.5 eV below the conduction band minimum). With the Cu level expected to be ~ 0.2 eV lower in energy than the native level, we can begin to assign the nature of the low energy PL we have observed. The change of ~ 0.12 eV of the low energy PL between the Cu mole percent of 5.5 to 15.2 implies that perhaps the initial Cu doping induces defects due to self-compensation. As the Cu ion is +1, for every two Cd ions it substitutes for, a Se vacancy would be needed for charge balancing purposes, until the stoichiometry of Cu_2Se was reached. So the large increase in the defect PL for low doped samples may arise from Se vacancies in the CdSe nanoparticle lattice. This would corroborate the low energy PL energy we observe, which is ~ 0.5 eV less than the BE PL. As the doping density is increased, the Cu levels dominate recombination centers and the low energy PL slowly redshifts. (see Figure 9) At the $x = 100$ limit (i.e. complete Cu substitution for Cd), we

arrive at the hypothetical CuSe_5 band gap of 0.7 eV, which is different than a previous report of the Cu_2Se band gap of 1.1 eV. [32] However, it should be noted that the Cu_2Se has a different crystal structure than CdSe and also has a complex defect structure which could affect our extrapolation. In addition, it is unknown how quantum confinement affects the electronic structure of Cu_2Se . However, by adding the CdSe confinement energy to the extrapolated CuSe_5 band gap, the value is $E_g = 1.06$ eV, within 4% of the value reported in Ref. 32.

4 Conclusions

In conclusion, we have studied the chemical composition and structure of a Cu substitutional impurity in CdSe nanocrystals. Using the elemental specificity of x-ray spectroscopy, we were able to identify the presence of Cu in the CdSe nanoparticle and assign it a +1 oxidation state. Inspection of Se L -edge x-ray absorption spectra indicated that the introduction of the more electronegative Cu ion into the lattice induced changes in the Se DOS, most likely due to changes in local bonding environment. The Se L -edge spectra provides evidence for statistical ion doping, as opposed to ion clustering. The introduction of Cu+1 lead to charge imbalances in the nanoparticle, which produced deep trap levels. Photoluminescence spectroscopy indicates that observed low energy PL is directly correlated to the Cu density.

5 Acknowledgments

This work was supported by the Office of Basic Energy Sciences, Division of Materials Science, under the auspices of the U.S. Department of Energy by the University of California, Lawrence Livermore National Laboratory under Contract No. W-7405-Eng-48. The work conducted at the Advanced Light Source is supported by the Director, Office of Science, Office of Basic Energy Sciences, Materials Sciences Division, of the U.S. Department of Energy under Contract No. DE-AC03-76SF00098 at Lawrence Berkeley National Laboratory. The authors thank Professor Pierre Petroff (UCSB) and Frederic Diana (UCSB) for the TEM images seen in this manuscript.

References

- [1] N.F. Johnson, *J. Phys.: Condens. Matter* **1997**, 7, 965.
- [2] A.P. Alivisatos, *J. Phys. Chem.* **1996**, 100, 13226.
- [3] M.L. Steigerwald, L.E. Brus, *Acc. Chem. Res.* **1990**, 23, 183.

- [4] S.A. Wolf, D.D. Awschalom, R.A. Buhrman, J.M. Daughton, S. von Molnar, M.L. Roukes, A.Y. Chtchelkanova, D.M. Treger, *Science* **2001**, 294, 1488.
- [5] R.N. Bhargava, *J. Lumin.* **1996**, 70, 85.
- [6] H. Mattoussi, J.M. Mauro, E.R. Goldman, G.P. Anderson, V.C. Sundar, F.V. Mikulec, M.G. Bawendi, *J. Amer. Chem. Soc.* **2000**, 122, 12142.
- [7] K.M. Hanif, R.W. Meulenberg, G.F. Strouse, *J. Amer. Chem. Soc.* **2002**, 124, 11495.
- [8] I. Broser, H. Maier, H.J. Schulz, *Phys. Rev.* **1965**, 140, 2135.
- [9] A.L. Robinson, R.H. Bube, *J. Appl. Phys.* **1971**, 42, 5280.
- [10] I.E. Türe, M. Claybourn, A.W. Brinkman, J. Woods, *J. Cryst. Growth* **1985**, 72, 189.
- [11] I.E. Türe, M. Claybourn, A.W. Brinkman, J. Woods, *J. Appl. Phys.* **1986**, 60, 1670.
- [12] S.B. Zhang, S.H. Wei, A. Zunger, *Phys. Rev. Lett.* **2000**, 84, 1232.
- [13] S.H. Wei, S.B. Zhang, A. Zunger, *J. Appl. Phys.* **2000**, 87, 1304.
- [14] S.B. Zhang, S.H. Wei, A. Zunger, *J. Appl. Phys.* **1998**, 83, 3192.
- [15] I.G. Dance, A. Choy, M.L. Scudder, *J. Am. Chem. Soc.* **1984**, 106, 6285.
- [16] O.E. Raola, G.F. Strouse *Nano Lett.* **2002**, 2, 1443.
- [17] S.L. Cumberland, K.M. Hanif, A. Javier, G.A. Khitrov, G.F. Strouse, S.M. Woessner, C.S. Yun, *Chem. Mater.* **2002**, 14, 1576.
- [18] M. Grioni, J.B. Goedkoop, R. Schoorl, F.M.F. de Groot, J.C. Fuggle, F. Schafer, E.E. Koch, G. Rossi, J.M. Esteve, R.C. Karnatak, *Phys. Rev. B* **1989**, 51, 17506.
- [19] H. Roulet, G. Dufour, A. Cheenne, F. Rochet, C. Cartier, *Appl. Surf. Sci.* **1991**, 47, 173.
- [20] J.F. Moulder, W.F. Stickle, P.E. Sobol, K.D. Bomben, in *Handbook of X-ray Photoelectron Spectroscopy*(Physical Electronics Inc.: Eden Prairie, 1995).
- [21] D.A. Zatsepin, V.R. Galakhov, M.A. Korotin, V.V. Fedorenko, E.Z. Kurmaev, S. Bartkowski, M. Neumann, R. Berger, *Phys. Rev. B* **1998**, 57, 4377.
- [22] W. Xiao, K. Xie, Q. Guo, E.G. Wang, *J. Phys.: Condens. Matter* **2003**, 15, 1155.

- [23] U. Fano, J.W. Cooper, *Rev. Mod. Phys.* **1968**, 40, 441.
- [24] M. Grioni, J.F. van Acker, M.T. Czyzyk, J.C. Fuggle, *Phys. Rev. B* **1992**, 45, 3309.
- [25] S. Hamza, S. Lewonczuk, J. Ringeissen, E. Beaurepaire, M.A. Khan, *Phys. Rev. B* **1995**, 51, 17506.
- [26] Y. Morita, M. Karppinen, H. Yamauchi, R.S. Liu, J.M. Chen, *J. Low Temp. Phys.* **2003**, 131, 1205.
- [27] A. Kobayashi, O. Sankey, S. Volz, J. Dow, *Phys. Rev. B* **1983**, 28, 935.
- [28] S. Pokrant, K.B. Whaley, *Eur. Phys. J. D* **1999**, 6, 255.
- [29] A. Wolska, R. Bacewicz, J. Filipowicz, K. Attenkofer, *J. Phys.: Condens. Matter* **2001**, 13, 4457.
- [30] M. Kuno, J.K. Lee, B.O. Dabbousi, F.V. Mikulec, M.G. Bawendi, *J. Chem. Phys.* **1997**, 106, 9869.
- [31] M.G. Bawendi, P.J. Carroll, W.L. Wilson, L.E. Brus, *J. Chem. Phys.* **1992**, 99, 946.
- [32] O.L. Bottecchia, *J. Braz. Chem. Soc.* **1998**, 9, 515.